Check for updates

Dome Collapse Interaction with the Atmosphere

Barfucci G. [1] and M. Ripepe[1]

[1] *Department of di Earth Sciences, University of Florence, Florence - Italy.*

Corresponding author: Giulia Barfucci (giulia.barfucci@unifi.it)

Key Points:

- Infrasonic and seismic amplitude of PDC allows forecasting the timing of final stage of the dome collapse.
- We show unprecedented observation of gravity waves associated with PDC episodes.
- We provide an estimation of the total erupted mass and the plume height during the Vulcanian explosions.

Accepted Article

This article has been accepted for publication and undergone full peer review but has not been through the copyediting, typesetting, pagination and proofreading process which may lead to differences between this version and the Version of Record. Please cite this article as doi: 10.1029/2018GL078243

© 2018 American Geophysical Union. All rights reserved.

Abstract

Dome collapse is a dramatic volcanic process which dynamics evolution still presents open questions. Observational data are rare and this limits our ability to interpret the evolution of this phenomenon in terms of risk assessment. We show how the partial dome collapse of Soufrière Hills Volcano on 2010 evolved in less than 45 minutes and was characterized by five main different episode of dome failure process. Time and amplitude of seismic and infrasonic records associated with successive pyroclastic density currents show a nearly quadratic temporal trend suggesting a self-accelerating process increasing in intensity up to the failure limit. Each episode generated gravity waves in the atmosphere, representing the first evidence of internal waves formed due to propagation of density currents in stratified fluids. Finally, we use gravity waves to estimate the total erupted mass and the plume height of the Vulcanian explosions triggered by the decompression induced by the collapse.

Plain Language Summary

Dome collapse is a dramatic and highly dangerous volcanic process involving the destabilization of large volume of hot material rushing as turbulent and destructive flows for kilometers down the flanks of the volcano. Dome collapse may trigger also large volcanic explosions that injecting a large amount of ash into the atmosphere constitute a serious risk for the air traffic. Dynamics of the dome instability still present open questions limiting our ability to assess the related hazard. Recent dome collapse reveals a strong interaction with the atmosphere. We show that collapse dynamics is able to induce buoyancy oscillations of the whole atmosphere generating gravity waves. These waves as linked to density currents were only theoretical predicted and this is the first evidence in natural environment. We show that the collapse evolved in five main steps lasting only 45 minutes and that forecast methods based on seismo-acoustic wavefield can be used to predict the end of the collapse. Finally we used the oscillation of the atmosphere to estimate the mass of ash injected and the plume height of the Vulcanian eruption triggered by the collapse.

Accepted Article

© 2018 American Geophysical Union. All rights reserved.

1 Introduction

Dome collapse episodes involve the mobilization of a great amount of juvenile material, due to gravitational instability or internal excess pressure within the dome itself. A dome collapse is always associated with pyroclastic density currents (PDCs) that move down the flanks of the volcano posing serious risks to local population. The large amount of ash dispersed in the atmosphere during the propagation of the PDC make direct visual observations of the collapse dynamics quite rare and, to date, poorly understood. Our ability to promptly assess the risk relies entirely on the correct interpretation of the data collected during the collapse and on our ability to understand whether or not the collapse is mainly driven by gravitational instability of dome faces or triggered by the increase of the internal magma pressurization (Sato et al., 1992). Unfortunately there are not many multiparametric networks which have recorded signals from dome collapse events.

The initial phase of most of the dome collapse is generally associated to intense seismicity, which is mainly related to large rockfalls and PDC activity (Luckett et al., 2007). Frequency content of seismic waves excited by this initial phase was, at Unzen volcano, explained in terms of different stages in PDC formation (Uhira et al., 1994). Sequential dome collapses at Merapi volcano show an interesting relation between seismic-amplitude envelopes area with the collapsing volumes (Brodscholl et al., 2000). This large movement of mass along the steep slopes of the volcano generates also infrasound (Yamasato, 1997*;* Oshima & Maekawa, 2001*;* Green and Neuberg, 2005) which has proved to be effective in detecting and tracking the evolution of PDC run out in real time (Ripepe et al., 2010, Delle Donne et al., 2014). Nevertheless, a detailed analysis of the infrasonic signal related to sustained PDCs production and dome collapse episode is still lacking.

The 11 February 2010 partial dome collapse at Soufrière Hills Volcano (SHV) was one of the largest since the eruption began in 1995 and produced approximately 5×10^7 m^3 of collapsed material from a total dome volume of ~25×10^7 m^3 (Stinton et al., 2014). The collapse occurred after a period of rapid lava extrusion and dome growth during January and February 2010, that generated block-and-ash flows, PDC events and a series of five Vulcanian explosions (Cole et al., 2014). The 11 February collapse event produced pyroclastic flows and high-energy surges followed by a strong Vulcanian explosive phase with a plume reaching ~12 km of elevation (Stinton et al., 2014).

Here, we present a detailed analysis of infrasonic and seismic records, which when integrated with images of the thermal camera, show how this dataset can be used to derive the evolution of the dome collapse. Infrasound and seismic amplitude grow with time following a quadratic

© 2018 American Geophysical Union. All rights reserved.

trend, which nicely fits the material failure law and allows forecasting the final stage of the collapse. Infrasound shows how the interaction between dome collapse and atmosphere generates an unprecedented record of gravity waves induced by PDCs activity. In addition, gravity waves are also clearly associated with the Vulcanian eruption and can be modeled to evaluate the total amount of volcanic ash injected into the atmosphere.

2 Instrumentation and Data Acquisition

The 11 February 2010 dome collapse at SHV has been recorded by seismic, infrasonic stations and thermal camera installed in cooperation with the Montserrat Volcano Observatory (MVO). A GURALP CMG-40T broad-band, three component seismometer, with eigenperiod of 30 s, was located at St. George's Hill (SGH) site at about 3 km from the active dome. The thermal camera and the infrasonic sensor were co-located at the Montserrat Volcano Observatory (MVO) at a distance of approximately 5.6 km from SHV. The camera is a FLIR A20 model equipped with 34° × 25° optical lens of 9.2 mm and a maximum thermal resolution of 0.1 °C in the 7.5–13 μm wavelength interval. The camera field of view (FOV) above SHV is approximately 3.5 × 2.5 km. The infrasonic sensor is a PRS100 (by iTEM) differential pressure transducer, with a sensitivity of 10 mV/Pa at 1 Hz, 250 Pa of full-scale range, a flat instrument response in the frequency band of 0.01–100 Hz, and a background noise level of 10^{-2}Pa. Seimic and infrasonic records have been corrected for each instrument response function.

3 Geophysical Observation of the Dome Collapse

The activity of Soufrière Hills Volcano on Montserrat, in the West Indies, is characterized by dome building phases of lava extrusion and episodes of partial or total dome collapses interspersed by Vulcanian explosions. Such explosive phases typically result from sudden decompression of the shallow magmatic system due to the lava dome disruption. Seismic and infrasonic stations on February 11, 2010 at 16:50 GMT recorded the beginning of a period of intense activity. Thermal imagery indicates that this activity coincides with a sequence of pyroclastic flows that released large quantities of ash in the atmosphere quickly covering the whole field of view (Figure 1). Thermal radiation, calculated by the integration of the temperature measured in the camera field of view (FOV) of each single frame, shows at 16:55 GMT a decay in the thermal intensity (Figure 1a). This thermal decay marks the

© 2018 American Geophysical Union. All rights reserved.

Accepted Article

beginning of a relative "cold" period, which follows the onset of the seismic and acoustic activity and is evidence of the beginning of an intense PDC phase. The quantity of ash dispersed in the atmosphere was large enough to make difficult the visual observation of the dome thus shielding the hot volcanic dome and reducing the total temperature in the camera field of view.

During this "cold" thermal period seismic and acoustic signals are characterized by comparable cigar-shape waveforms with the gradual increase-decrease of the amplitude (Figure 1 d, e). The similarity between seismic and infrasonic waveforms is compatible with a source moving at the interface between the ground and the atmosphere typical of mass movements such as density currents (e.g. De Angelis et al., 2007; Ripepe et al., 2010).

Despite the strong similarity in the waveforms, seismic and infrasonic signals have a different frequency content, whereas seismic signal shows a broad frequency content above 0.1 Hz, infrasound shows a remarkably wide spectrum ranging from 1mHz up to a few hertz (Figure 2b). However, above 0.1 Hz, seismic signal reaches the maximum amplitude at around 1-4 Hz, typical of PDC (Uhira et al., 1994; De Angelis et al., 2007) whereas infrasound is charcterized by a much lower frequency content around 0.4 Hz. In spite of the similar cigar-shape waveform, this different frequency content indicates that the energy during the propagation of the PDCs is differently partitioned. While seismic waves are driven by the friction of the sliding source with the ground, infrasound is associated to the displacement of the atmosphere during the movement.

This activity indicate that the gravitational process of the unstable dome collapse is characterized by a sequence of at least five major PDC episodes with peak amplitude at 16:56, 17:06, 17:10, 17:14, 17:16 GMT.

At the end of this period, at 17:20:15, strong impulsive signals in the seismic and acoustic record coincide with two high temperature impulses in thermal radiation (Figure 1), and mark the onset of two large Vulcanian explosions.

At 17:35:00, only 45 minute after the beginning of a dome collapse, all the geophysical parameters drop back to a pre-activity level marking the end of the dome collapse.

Accepted Article

© 2018 American Geophysical Union. All rights reserved.

4 Gravitational Dome Instability and the Materials Failure Law

Signal amplitude associated with the five PDC episodes increases with time (Figure 1 and 3), both in the infrasound (from 2.5 to 8 Pa recorded at 5.6 km from the source and high-pass filtered >0.1 Hz) and in the seismic (from $2x10^{-3}$ to $5.7x10^{-3}$ m/s). These indicate that the collapse evolved through 5 major steps of incrementally larger episodes of flank instability (Figure 1) over a period of half an hour (from 16:50 to 17:20). While the duration of each event decreases from ~300 s to ~60 s, the rate of occurrence is increasing with time (Figure 3).

This pattern in amplitude and PDCs rate suggests a self-accelerating process that increases in intensity up to a critical point (Figure 3). Similar behavior has been originally observed with regard to materials in terminal stages of failure (Fukuzono & Terashima, 1982) and it was then successfully extended also to the eruption processes at volcanoes as an analytical basis for eruption prediction (Voight, 1988). The empirical relation driving the mechanics of failure reads as:

$$\ddot{\omega} = C\dot{\omega}^{\alpha} \tag{1}$$

where C and α are two empirical constants and ω is the observed geophysical quantity. Concerning eruption processes, behavior of some of the observable parameters, preceding a volcanic eruption, can be described by this physical law (Voight, 1988; Hammer and Neuberg, 2009). The material failure forecast method has been applied to the observed pattern of seismic energy released before the eruption and to the deformation of the summit at Merapi volcano and it proved to be able to forecast the eruption time with good accuracy (Budi-Santoso et al., 2013). In all these studies, the empirical constant α is found to be frequently nearly 2. Integrating equation (1) for $\alpha > 1$ and with boundary condition $\dot{\omega}(t_f) = \dot{\omega}_f$, where t_f *is* the time of failure (see Voight 1988, for details), we derive the following expression for the rate $\dot{\omega}$ of the observed geophysical quantity:

$$\dot{\omega}_i = \left[C(\alpha - 1)(t_f - t_i) + \dot{\omega}_f^{1-\alpha}\right]^{1/(1-\alpha)} \tag{2}$$

which for $\alpha = 2$ becomes:

$$\dot{\omega}_i^{-1} - \dot{\omega}_f{}^{-1} = C(t_f - t_i) \tag{3}$$

where the inverse rate of the observed geophysical quantity $\dot{\omega}^{-1}$ decreases linearly with time.

© 2018 American Geophysical Union. All rights reserved.

Accepted Article

In our case we set $\dot{\omega}_i^{-1} = (T_i - T_{i-1})/(A_i - A_{i-1})$ as the inverse rate of the amplitude increase of the seismic (Figure 3a) and infrasonic (Figure 3b) signals related to the five PDCs, as predicted by the failure law (equation (3)), the observed trends show an inverse linear rate with time (Figure 3).

In analogy with the failure time of materials, a "*critical time*" for the observed process can be estimated as the time the inverse rate goes to zero (Voight, 1988). In our case we estimate that the "*critical time*", t_c, will occur between 17:16:24 and 17:16:50, with a best fit of R^2=0.98 and only ~3.5 minutes before the onset of the vulcanian explosion occurred at 17:20:15 (Figure 3). Considering 95% confidence intervals, these critical times t_c can have a variability of no more than +|- 3 min for both the seismic and infrasonic amplitude variation. The use of the failure law allows evaluating when the dome collapse will end and for how long it will last.

5 Atmospheric Gravity Waves of PDC

Pressure signals recorded during the dome collapse are characterized by large, long-period, oscillations, visible also in the raw data (Figure 1). Spectral analysis reveals these oscillations have broad frequency content, ranging from 0.01 Hz to 1 mHz (Figure 2b). A significant proportion of the acoustic energy is thus concentrated below the typical frequency content of infrasound (>0.1 Hz) and it is breaking the limit (3.0 mHz for a standard atmosphere) of the propagation of acoustic waves. Below the acoustic cut-off frequency, pressure oscillations are dominated by the gravity term, and pressure propagates as gravity wave, while just above, wave propagation is controlled by the elastic properties of the atmosphere. Acoustic and gravity waves are commonly observed in the ocean where they are decoupled, but both waves can propagate as coupled acousto-gravity waves in the atmosphere (Gossard and Hooke, 1975).

Pressure signal filtered above the cut-off frequency shows oscillations peaking at around 4 mHz frequency content, typical of acousto-gravity waves, which present shared features between pure acoustic waves, dominated by elasticity of the atmosphere, and gravity waves controlled by buoyancy effects. Gravity waves (Figure 2a) become clear by filtering below the cut-off frequency and are characterized by oscillations of increasing amplitude, from 3 to 9 Pa while approaching the explosive phase at 17:20:15. It is worth noting that both acoustic-gravity and gravity waves, only appear after the emplacement of the first PDC at 16:50 GMT. Besides, these waves appears well phased with the amplitude modulation of the seismic and

© 2018 American Geophysical Union. All rights reserved.

Accepted Article

infrasonic signal produced by the five PDC episodes (Figure 1c-e). We thus infer that these oscillations may represent the reaction of the atmosphere to the air displacement that each current produces by propagating along the flanks of the volcano.

Gravity waves induced by propagation of a density current in a stratified medium have been studied in relation to small-scale laboratory experiment and are predicted by numerical modeling (Simpson, 1997). However, observations, and records, of these waves induced by density currents in nature are to date rare, and this is the first record of gravity waves associated with strong PDCs activity and dome collapse.

6 Eruptive Source Parameters of Vulcanian Explosion

Thermal camera, seismic and infrasonic records show (Figure 1) that gravitational instability of the dome ends at ~17:20 interrupted by a violent Vulcanian explosion. Relative thermal intensity calculated by integrating the camera field of view above the 30°C treshold (Figure 1) indicates at least two clear thermal pulses at 17:20:14 and 17:21:40, lasting 74 and 42 seconds, respectively, which seems associated with two acoustic peaks at 41 and 28 Pa, respectively. Evidence of at least two pulses during the explosive phase were also reported by Cole et al., in 2015, on the base of thermal recordings. The explosive injection of mass and thermal energy into the atmosphere have triggered gravity waves which amplitude increases to higher values (up to 22 Pa, Figure 2a) with respect to those observed during the PDCs activity (Figure2). In case on volcanic eruptions, duration and frequency content of gravity waves are in general better explained by the addition of mass than of thermal energy in the atmosphere (Baines & Sacks, 2014). Therefore, we assume a point source located in the atmosphere above the ground to model gravity waves as the convolution $P(x,t) = \dot{q}(t) * h(x,t)$ between the oscillation of the free atmosphere $h(x, t)$ and the first derivative of the mass flow rate $\dot{q}(t)$ (Kanamori et al., 1994). Here, the oscillation of the atmosphere, $h(x, t)$, is calculated as the response of the atmosphere in m^{-1} to the unitary step of the mass flow rate recorded at a distance x from the source (Kanamori et al., 1994) and for a given atmospheric profile at the time of the eruption (e.g. Ripepe et al., 2016). Location of the source represents the elevation at which the transition between the gas thrust (momentum) and the buoyancy regime in the plume dynamics occurs.

We assume here that the source time function is described by the exponential source function generally used to represent the mass flow rate, $q(t)$, (Mikumo & Bolt, 1985; Kanamori et al., 1994; Ripepe et al., 2016), (Figure 4):

© 2018 American Geophysical Union. All rights reserved.

Accepted Article

$$q(t) = Q_o \frac{t}{\tau}\left(1 - \frac{t}{\tau}\right) \quad (4)$$

where Q_o is the maximum mass eruption rate and τ is the rise time of the source in seconds. The best fit of R^2=0.85 with the observed pressure wave is calculated considering all the possible elevation of the source between the sea level and 9000 m, and a rise time (τ) changing in the 2 – 400 s range (Figure 4). Considering all the solutions with R^2>0.8 the source is located at an elevation of 4650±300m a.s.l., has a rise time, τ, of 21.6±0.9 s, (Figure 4c) and a total duration of the mass pulse of ~120 s, which is in agreement with the duration of ~130 seconds of the two thermal pulses (~80 and ~50 seconds each). Our modeling shows that amplitude of the gravity waves is compatible with a maximum mass eruption rate Q_o of 1.2±0.3x10^8 kg/s, which integrated over the source time function gives a total erupted mass of 5.7±0.5 x 10^9 kg.

Total erupted mass can be converted into plume height, using the relationship for the Earth's standard atmosphere $H = 0.042M^{1/4}$ (Parfitt & Wilson, 2008) where *M* is the total mass of solids and gas ejected and, *H* is the plume height in kilometers which in our case is 11.5±0.3 km. Gravity waves generated during the five PDCs episodes probably were still exciting oscillations in the atmosphere when vulcanian explosion occurred. This means that the gravity waves we modeled could have been contaminated by oscillation of the atmosphere started before the explosive onset. The two gravity wavefields, before and after the explosion (Figure 4a), have very similar frequency content and thus the contribution of the PDC-induced gravity waves can not be easily separated from the vulcanian-related ones, with non quantified effects on our modeling However, the good fit of R^2=0.85 between observation and model seems suggesting that if there was a contamination this would have been probably very low.

7 Discussion and Conclusions

Dome collapse is a rare and dramatic event in the dynamic evolution of volcanic activity. In Montserrat the 1995 collapse of the SHV dome had a large impact on the economy and life of the island causing the complete destruction of the capital Plymouth, the commercial harbor and the international airport. Besides the high risk related to the collapse, there are still open questions regarding the evolution of these phenomena also because observational data are still rare. Data presented in this work represent an almost unique geophysical dataset, used here to identify the major steps leading to the collapse of the SHV dome that occurred on February 11, 2010.

© 2018 American Geophysical Union. All rights reserved.

Accepted Article

The collapse was characterized by five large PDC episodes, each of them associated to different steps in the progressive failure of the dome. Waveforms of seismic and infrasonic signals are consistent with a moving source differently coupled with the ground and the atmosphere. We show how while the amplitude of seismic and infrasonic signal is increasing, the temporal separation of the PDCs episodes decreases following a nearly quadratic trend. This is remarkably well-explained by the material failure law (Fukuzono & Terashima, 1982; Fukuzono, 1985) indicating that the collapse was controlled by the progressive self-accelerating gravitational instability. More observations might clarify whether and how mechanisms underlying dome collapse may be described by deterministic models. However, our results indicate that seismic and infrasonic amplitude in case of gravitational instability of the dome may follow a well-defined pattern, which can be used to forecast the final stage of the dome collapse. The possibility to estimate the duration of the ongoing collapse would represent an important parameter to evaluate the risk exposure of human lives and/or goods to PDCs activity, with immediate impact on the risk management.

Besides, while seismic waves do not show any significant change in the frequency content, infrasound shows that pyroclastic episodes are characterized by a peak frequency content around

0.4 Hz. Frequency content of PDC is lower than what previously observed for PDC activity at SHV (1-2 Hz, see Ripepe et al., 2010). Considering that these events are bigger than those analyzed in 2008 this seem suggesting that a relationship between the frequency of the acoustic signal and the size of the PDC might exist.

The large volume of material displaced is responsible for unprecedented observation of gravity waves (<0.003 Hz) and acousto-gravity waves associated with dome failure and/or the large quantity of thermal heat released during the intense pyroclastic flow activity. Our observations indicate for the first time that the PDCs activity is able to perturb the atmosphere inducing gravity waves. Numerical simulation and experimental studies also at smaller scale indicate that internal waves can be formed due to propagation of density currents in stratified ambient (Birman et al., 2007, Amen & Maxworthy, 1980) and have proved that such waves can heavily affect the kinematic parameters of the current (Maxworthy et al., 2002). However observations and records of these waves induced by density currents in natural environments are still rare. Continuous records of such waves may provide new insight on the interaction of gravitational instability phenomenon with the atmosphere and may represent a starting point for future works on density currents

Accepted Article

© 2018 American Geophysical Union. All rights reserved.

propagating in stratified fluids in comparison with experimental studies and computational models.

The 30 minutes long gravitational instability steps of the dome collapse has most probably induced a magma decompression responsible for two violent vulcanian explosions reaching ~12 km of height. The response of the atmosphere to the injection of the volcanic mass generated one hour long gravity waves. Modeling of these gravity waves (Kanamori et al., 1994; Ripepe et al., 2016) is compatible with a point mass injection source located at 4600 m a.s.l. lasting 120 seconds. The best misfit between data and model (R^2=0.85) is achieved for a total DRE ejected mass of $5.7\pm0.5 \times 10^9$ kg, which corresponds to a plume height of ~11.5 km. At the end, the total duration of the collapse lasted 45 minutes inducing decompression on the magmatic system only after 30 minutes and generating gravity perturbation in the atmosphere.

Acknowledgments

We are grateful to Montserrat Volcano Observatory (MVO) staff for technical support in the field and to Dario Delle Donne and Giorgio Lacanna for sharing data and experience with us. This manuscript has been improved by the critical comments of David Green and anonymous Reviewer. The authors comply with AGU's data policy and seismic and infrasonic data used to achieve most of the findings and create most of the figures are available as supporting information.

Accepted Article

© 2018 American Geophysical Union. All rights reserved.

References

Amen, R. and T. Maxworthy (1980), The gravitational collapse of a mixed region into a linearly stratified fluid, J. Fluid Mech. 96, 65–80.

Baines, P.G. and S. Sacks (2014), Atmospheric internal waves generated by explosive volcanic eruptions, in: The Eruption of Soufrière Hills Volcano, Montserrat from 2000 to 2010, edited by: Wadge, G., Robertson, R. E. A., and Voight, B., Geological Society, London, Memoirs, 39, Geological Society: London, UK, Volume 39, pp. 153–168.

Baines, P.G. and S. Sacks (2017), The Generation and propagation of atmospheric internal waves caused by volcanic eruptions, Atmosphere, 8(3), 60; doi:10.3390/atmos8030060

Birman, V. K., Meiburg, E. and M. Ungarish (2007), On gravity currents in stratified ambients, Phys. Fluids, **19**, 086602.

Budi-Santoso, A., Lesage, P., Dwiyono, S., Sumarti, S., Subandriyo, Surono, Jousset, P. and JP. Metaxian (2013), Analysis of the seismic activity associated with the 2010 Eruption of Merapi Volcano, Java, J. Volcanol. Geotherm. Res., 261: 153–170. doi:10.1016/j. j.jvolgeores.2013.03.024

Cole, P. D., Smith, P. J., Stinton, A. J., Odbert, H. M., Bernstein, M. L., Komorowski, J. C. and R. Stewart (2014), Vulcanian explosions at Soufrière Hills volcano, Montserrat between 2008 and 2010, in: The Eruption of Soufrière Hills Volcano, Montserrat from 2000 to 2010, edited by: Wadge, G., Robertson, R. E. A., and Voight, B., Geological Society, London, Memoirs, 39, 93–109, http:// dx.doi.org/10.1144/M39.5

Cole, P.D., Stinton, A. J., Odbert, H. M., Bonadonna, C., and R. C. Stewart (2015), An inclined Vulcanian explosion and associated products, Journal of the Geological Society, 172, 287-293, https://doi.org/10.1144/jgs2014-099

De Angelis, S., Bass, V., Hards, V. and G. Ryan (2007), Seismic characterization of pyroclastic flow activity at Soufrière Hills Volcano, Montserrat, 8 January 2007, Nat. Hazards Earth Syst. Sci., 7, 467–472.

Delle Donne, D., Ripepe, M., De Angelis, S., Cole, P. D., Lacanna, G., Poggi, P., and R. Stewart (2014), Thermal, acoustic and seismic signals from pyroclastic density currents and vulcanian explosions at Soufrière Hills Volcano, Montserrat, in: The Eruption of Soufrière Hills Volcano, Montserrat from 2000 to 2010, edited by: Wadge, G., Robertson, R. E. A., and Voight, B., Geological Society, London, Memoirs, **39**, 169–178

Fukuzono, T. (1985), in Proc. 4th Natl. Conf. Field Workshop on Landslide, 145-150, Disaster Research Institute, Kyoto.

Accepted Article

© 2018 American Geophysical Union. All rights reserved.

Fukuzono, T. and H. Terashima (1982), H. Rep. Natn. Res. Center Disaster Prev. 29, 103-122.

Green, D. N., and J. Neuberg (2005), Seismic and infrasonic signals associated with an unusual collapse event at the Soufrière Hills volcano, Montserrat, Geophys. Res. Lett., 32, L07308, doi:10.1029/2004GL022265.

Gossard, E.E. and W.H. Hooke (1975), Waves in the Atmosphere, Elsevier, New York.

Hammer, C. and J.W. Neuberg (2009), On the dynamical behaviour of low- frequency earthquake swarms prior to a dome collapse of Soufriere Hill volcano, Montserrat, Geophys. Res. Lett., **36.**

Kanamori, H., J. Mori, and D. G. Harkrider (1994), Excitation of atmospheric oscillations by volcanic eruptions, J. Geophys. Res., 99, B11, 21947-21961.

Luckett, R., Baptie, B., Ottemoller, L., and G. Thompson (2007), Seismic Monitoring of the Soufrière Hills Volcano Montserrat, Seism. Res. Lett., 78(2), 192–200.

Maxworthy, T., Leilich, J., Simpson, J. E. and E.H. Meiburg (2002), The propagation of a gravity current into a linearly stratified fluid, Journal of Fluid Mechanics, 453, 371–394.

Mikumo, T. and B.A. Bolt (1985), Excitation mechanism of atmospheric pressure waves from the 1980 Mount St Helens eruption. Geophys. J. Int. **81,** 445–461.

Oshima H. and T. Maekawa (2001), Excitation process of infrasonic waves associated with Merapi-type Pyroclastic Flow as Revealed by a new recording system, Geoph. Res. Lett., 28(6), 1099-1102.

Parfitt, E. A. and L. Wilson (2008), In Fundamentals of Physical Volcanology, Blackwell, Cambridge, Mass.

Ripepe, M., De Angelis, S., Lacanna, G. and B. Voight (2010), Observation of infrasonic and gravity waves at Soufrière Hills Volcano, Montserrat, Geophys. Res. Lett. **37,** L00E14, doi: 10.1029/2010GL042557.

Ripepe, M., Barfucci, G., de Angelis, S., delle Donne, D., Lacanna, G. and E. Marchetti (2016), Modeling volcanic eruption parameters by near-source internal gravity waves, Sci. Rep., 6, 26727.

Sato, H., Fujii, T. and S. Nakada (1992), Crumbling of dacite dome lava and generation of pyroclastic flows at Unzen volcano, Nature, 360, 664-666.

Accepted Article

© 2018 American Geophysical Union. All rights reserved.

Simpson, J. E. (1987), Gravity currents in the environment and the laboratory, 2nd ed. Cambridge University Press.

Stinton, A. J., Cole, P. D., Stewart, R.C., Odbert, H.M. and P. Smith (2014), The 11 February 2010 partial dome collapse at the Soufrière Hills Volcano, Montserrat. In: The Eruption of Soufrière Hills Volcano, Montserrat, from 2000 to 2010, edited by: Wadge, G., Robertson, R. E. A., and Voight, B., Geological Society, London, Memoirs, 39, 111- 129.

Yamasato, H. (1997), Quantitative analysis of pyroclastic flows using infrasonic and seismic data at Unzen Volcano, Japan, J. Phys. Earth, 45, 397-416.

Uhira, K., H. Yamasato, and M. Takeo (1994), Source mechanism of seismic waves excited by pyroclastic flows observed at Unzen volcano, Japan. J. Geophys. Res., 99, 17757-17773.

Voight, B. (1988), A method for prediction of volcanic eruptions, Nature, 332, pp. 125-130.

Accepted Article

© 2018 American Geophysical Union. All rights reserved.

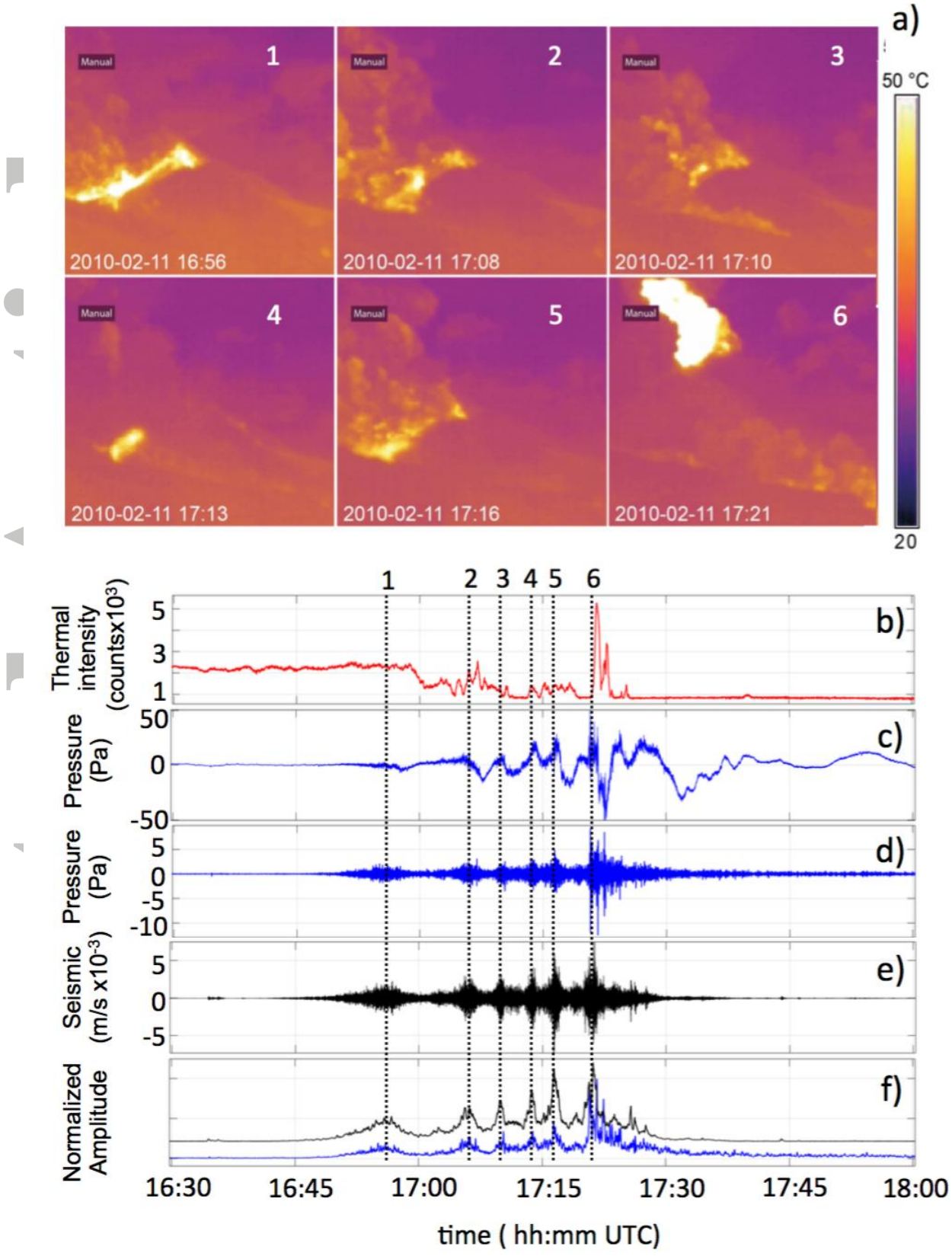

Figure 1. Synoptic view of the geophysical dataset collected during the dome collapse. (a) Frames showing the six different phases of the collapse; (b) number of pixels above the temperature threshold of 30°C is used as proxy of the frame-by-frame thermal intensity detected in the camera field of view; (c) acoustic record raw and (d) high–pass filtered 0.1

© 2018 American Geophysical Union. All rights reserved.

Hz; (e) seismic ground velocity and (f) envelope of seismic (black) and infrasonic (blue) amplitude. Infrasonic and seismic signals show five major steps of the collapse. These steps (from 1 to 5) correspond to the PDC episodes, with seismic and infrasonic increasing amplitude with time. The last step (#6) indicates the onset of the vulcanian explosions occurred at 17:20:15 GMT at the end of the dome collapse.

Accepted Article

© 2018 American Geophysical Union. All rights reserved.

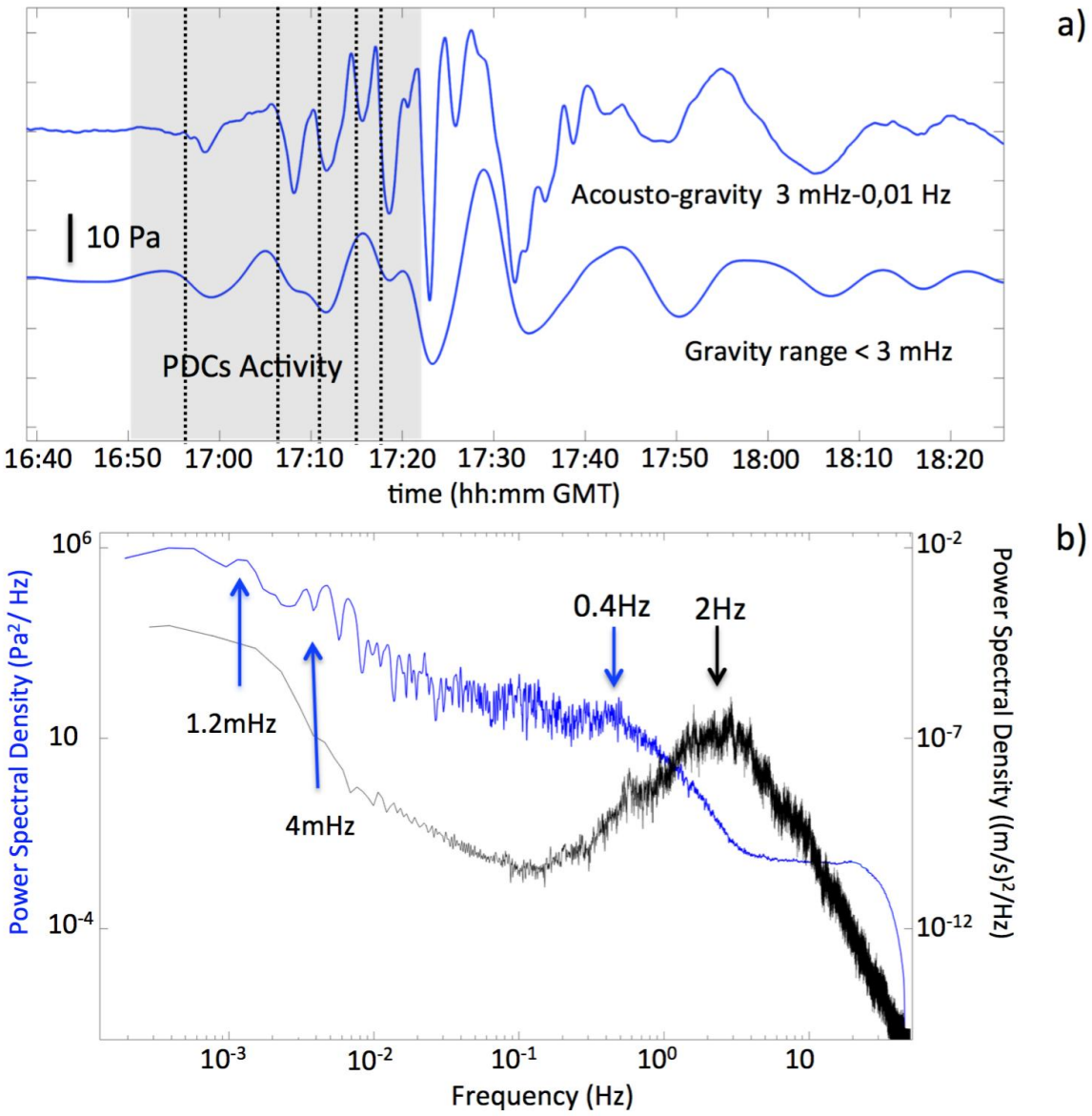

Figure 2. (a) Acoustic record once corrected for the instrument response function is filtered (up) in the acousto-gravity range between 3mHz and 0.01 Hz and is low-pass filtered (down) in the gravity waves band below 3 mHz. Dashed lines indicate the occurrence of the five PDC episodes of Figure 1; (b) Power Density Spectra of seismic (black line) and infrasonic (blue line) signals show that the energy released during the PDC events is differently partitioned between seismic and acoustic waves.

Accepted

© 2018 American Geophysical Union. All rights reserved.

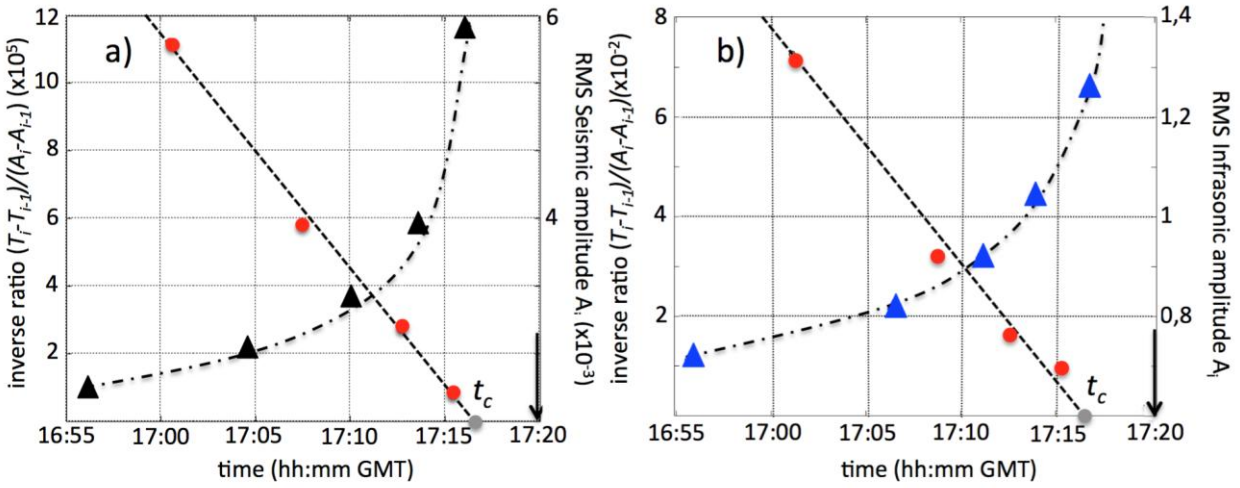

Figure 3. RMS of (a) seismic and (b) infrasonic amplitude and their inverse rate of the amplitude increase (red circles). Inverse rate of the amplitude is decreasing following a linear fit (dashed line) of, R^2 =0.98, both for the seismic and infrasonic data. The gray dots indicate the critical time, t_c, and the arrows the onset of the vulcanian explosions.

Accepted Article

© 2018 American Geophysical Union. All rights reserved.

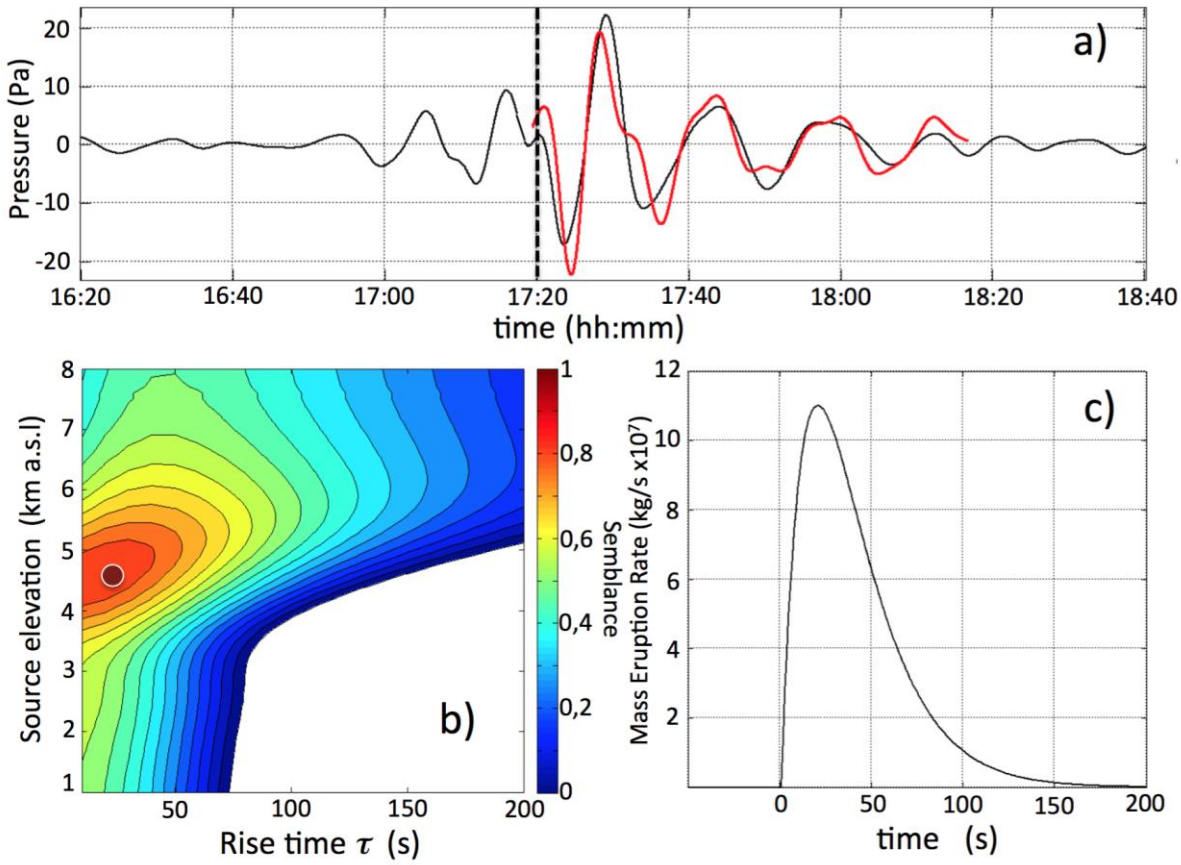

Figure 4. (**a**) Gravity waves recorded (black line) and calculated (red line) using the point mass injection source model. Dashed line represents the onset of the Vulcanian explosion and the onset of the modeling. (**b**) Close up of the semblance map between the measured and the modeled gravity waves for different source elevations and rise times. Red dot indicates the best solution of $R^2 = 0.85$. (**c**) Mass eruption rate associated with the best fit and relative to the gravity waves (red line) shown in panel (a).

Accepted

© 2018 American Geophysical Union. All rights reserved.